AGU PUBLICATIONS

JGR

Journal of Geophysical Research: Space Physics

RESEARCH ARTICLE
10.1002/2015JA022252

Special Section:
Big Storms of the Van Allen Probes Era

Large-amplitude electric fields in the inner magnetosphere: Van Allen Probes observations of subauroral polarization streams

S. Califf[1], X. Li[1], R. A. Wolf[2], H. Zhao[1], A. N. Jaynes[1], F. D. Wilder[1], D. M. Malaspina[1], and R. Redmon[3]

[1]Laboratory for Atmospheric and Space Physics, University of Colorado Boulder, Boulder, Colorado, USA, [2]Department of Physics and Astronomy, Rice University, Houston, Texas, USA, [3]National Geophysical Data Center, NOAA, Boulder, Colorado, USA

Abstract The subauroral polarization stream (SAPS) is an important magnetosphere-ionosphere (MI) coupling phenomenon that impacts a range of particle populations in the inner magnetosphere. SAPS studies often emphasize ionospheric signatures of fast westward flows, but the equatorial magnetosphere is also affected through strong radial electric fields in the dusk sector. This study focuses on a period of steady southward interplanetary magnetic field (IMF) during the 29 June 2013 geomagnetic storm where the Van Allen Probes observe a region of intense electric fields near the plasmapause over multiple consecutive outbound duskside passes. We show that the large-amplitude electric fields near the equatorial plane are consistent with SAPS by investigating the relationship between plasma sheet ion and electron boundaries, associated field-aligned currents, and the spatial location of the electric fields. By incorporating high-inclination DMSP data we demonstrate the spatial and temporal variability of the SAPS region, and we suggest that discrete, earthward propagating injections are driving the observed strong electric fields at low L shells in the equatorial magnetosphere. We also show the relationship between SAPS and plasmasphere erosion, as well as a possible correlation with flux enhancements for 100s keV electrons.

Key Points:
- SAPS electric fields are shown in relation to equatorial magnetospheric particle boundaries
- RBSP and DMSP observations suggest that SAPS region is composed of numerous earthward propagating spatial structures
- SAPS electric fields are correlated with plasmasphere erosion

Correspondence to:
S. Califf,
califf@colorado.edu

Citation:
Califf, S., X. Li, R. A. Wolf, H. Zhao, A. N. Jaynes, F. D. Wilder, D. M. Malaspina, and R. Redmon (2016), Large-amplitude electric fields in the inner magnetosphere: Van Allen Probes observations of subauroral polarization streams, *J. Geophys. Res. Space Physics*, *121*, 5294–5306, doi:10.1002/2015JA022252.

Received 7 DEC 2015
Accepted 20 MAY 2016
Accepted article online 23 MAY 2016
Published online 17 JUN 2016

1. Introduction

Subauroral polarization streams (SAPS) [*Foster and Burke*, 2002] play an important role in modifying the electric field in the equatorial inner magnetosphere, contributing to a region of intense electric fields in the dusk sector. SAPS are typically discussed from an ionospheric point of view as a strong westward plasma flow equatorward of the auroral precipitation boundary commonly occurring between dusk and predawn [*Foster and Vo*, 2002]. The westward flow corresponds to a poleward electric field in the ionosphere, which maps to the equatorial magnetosphere as a radially outward electric field.

SAPS arise from coupling between the magnetosphere and the ionosphere, and the location and intensity of the flow depend on numerous factors, including plasma sheet particle precipitation boundaries, magnetospheric pressure gradients, field-aligned currents, and ionospheric conductivity [e.g., *Southwood and Wolf*, 1978; *Anderson et al.*, 2001]. During periods of enhanced convection, plasma sheet ions and electrons are transported from the tail into the inner magnetosphere. Due to the combination of convection, corotation, and oppositely directed gradient drifts for ions and electrons, the inner edge of the plasma sheet ions is earthward of the inner edge of the plasma sheet electrons of similar energy on the duskside [e.g., *Korth et al.*, 1999].

Pressure gradients at the inner edge of the plasma sheet ions can lead to Region 2-type field-aligned currents that flow into the ionosphere equatorward of the precipitating electron boundary and close poleward (Figure 1). In the absence of sunlight, ionospheric conductivity is driven mainly by precipitating electrons [e.g., *Burke et al.*, 1998], so the current closes through a region of low conductivity between midnight and dusk, leading to a strong poleward electric field in the ionosphere. Additionally, the increased flow speed in the ionosphere leads to frictional heating and increased recombination rates, which can further decrease the conductivity and create a positive feedback effect on the SAPS electric field [*Schunk et al.*, 1976; *Banks and Yasuhara*, 1978].

This study focuses on a period of steady southward IMF in late June 2013 where the Van Allen Probes observe strong electric fields spanning the outer edge of the plasmasphere on multiple duskside passes. We investigate the relationship between the electric field and particle measurements in the equatorial inner magnetosphere during this 18 h period, and we complement the observations with high-inclination data

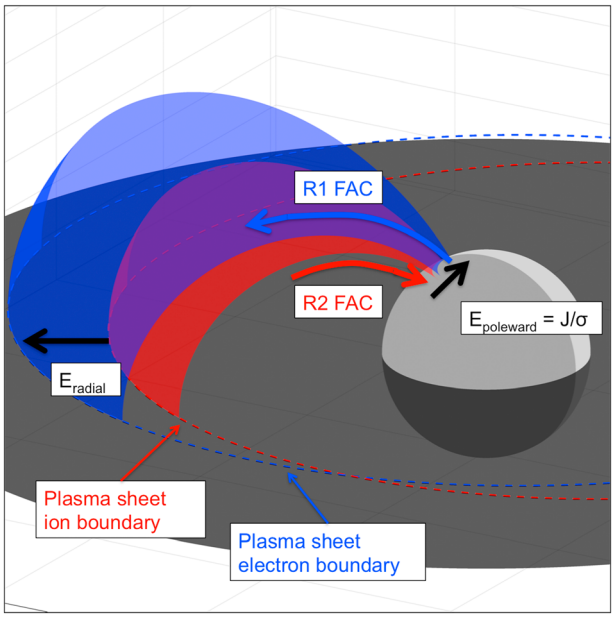

Figure 1. Diagram of field-aligned currents flowing into the ionosphere at the inner edge of the plasma sheet ions, which is equatorward of the plasma sheet electrons near dusk. The current closes poleward through a low-conductivity region, causing the strong SAPS electric field that maps to the equatorial magnetosphere.

from DMSP. Previous studies comparing equatorial and high-latitude data have focused on magnetically conjugate observations of latitudinally narrow subauroral ion drift (SAID) events [e.g., *Burke et al.*, 2000; *Puhl-Quinn et al.*, 2007]. In contrast, our study provides a broad overview of the evolution of the SAPS region and its impact on the inner magnetosphere from an equatorial perspective over the course of a long-lasting geomagnetic storm, with concurrent supporting measurements from high latitude as well. The data suggest that SAPS can be characterized as a broad spatial region persisting for hours that also contains smaller-scale spatial and temporal variation due to numerous earthward propagating injections. We also show that the SAPS electric field is correlated with plasmasphere erosion and 100s keV electron enhancements deep within the inner magnetosphere.

2. Event Overview

On 27 June 2013, a coronal mass ejection (CME) arrived at Earth, causing a geomagnetic storm with minimum $Dst < -100$ nT that lasted for several days. Figure 2 shows the solar wind conditions and geomagnetic indices for the storm. Initially, there was an increase in dynamic pressure from a combination of higher solar wind speed and density in the CME, and then early on 28 June the interplanetary magnetic field (IMF) began to turn southward, which is a signature of a magnetic cloud event [e.g., *Kataoka et al.*, 2015]. The IMF remained steadily southward for 18 h (Figure 2a, dashed lines), and during this period there was increased substorm activity, as indicated by the elevated *AE* index (Figure 2e). The *Dst* index reached −100 nT during the long-duration main phase, and *Dst* remained below −70 nT until the IMF abruptly turned northward, initiating a slow recovery over the next two days. During the interval of steady southward IMF, the Van Allen Probes observed large-amplitude DC electric fields spanning ~1 R_E in radial distance over four consecutive outbound passes across the duskside inner magnetosphere. We focus on the cause of the strong

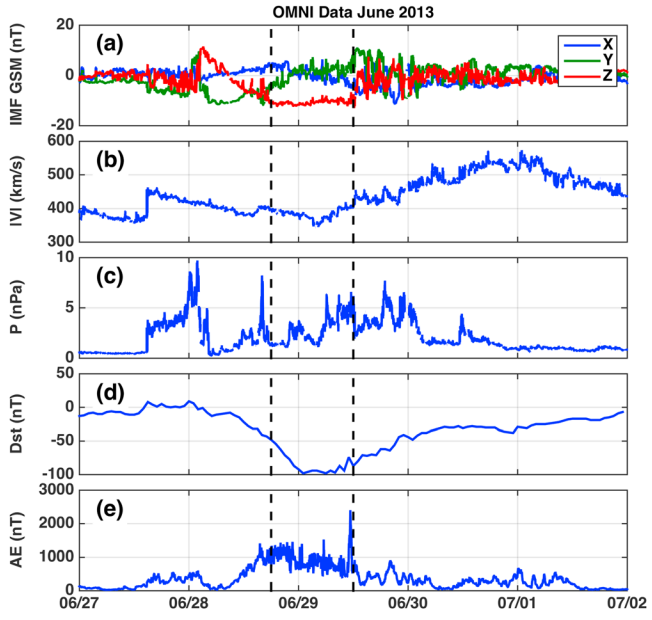

Figure 2. Solar wind conditions and geomagnetic indices for the 27 June 2013 geomagnetic storm. (a) Interplanetary magnetic field, (b) solar wind speed, (c) solar wind pressure, (d) *Dst* index, and (e) *AE* index.

electric fields by investigating their relationship to plasma sheet particle boundaries and field-aligned currents both near the equatorial plane and at high latitudes.

3. Data Description

The equatorial data are from the twin Van Allen Probes, which are in approximately geotransfer orbits with ~10° inclination. The magnetic latitude of the observations varies between ±20° due to the tilted offset of the Earth's dipole, and the spacecraft typically cover all L shells up to $L \sim 6$ depending on magnetic latitude, although in some cases the L shell can reach $L > 12$ in the midnight sector [e.g., *Saikin et al*., 2015]. During the 29 June 2013 time period, both spacecraft have apogees near 21 MLT, and the outbound portion of the orbit provides a radial cut of the equatorial magnetosphere between 18 and 21 MLT, which is ideal for observing the duskside SAPS feature. The orbital periods are 9 h, and the spacecraft are separated by approximately 4 h during this time. We focus on consecutive outbound passes that provide a radial spatial profile of the electric field, plasma sheet particle boundaries, and field-aligned currents between $L = 2$ and 6. We use DC electric field data from the Electric Field and Waves (EFW) experiment [*Wygant et al*., 2013] expressed in the frame corotating with Earth. EFW also provides a measurement of spacecraft potential, which has been calibrated to estimate density through comparison with the density derived from the upper hybrid line [*Kurth et al*., 2015]. We use EFW density primarily to identify the plasmapause. To infer currents, we use fluxgate magnetometer data from Electric and Magnetic Field Instrument and Suite and Integrated Science (EMFISIS) [*Kletzing et al*., 2013], and the ion and electron observations are provided by Helium, Oxygen, Proton, and Electron (HOPE) [*Funsten et al*., 2013] for energies up to ~50 keV and Magnetic Electron Ion Spectrometer (MagEIS) [*Blake et al*., 2013] for 50 keV to MeV energies.

To complement the Van Allen Probes observations, we use low-altitude, high-inclination data from DMSP F16, F17, and F18, which are in ~800 km Sun-synchronous polar orbits. We use differential particle fluxes from the Special Sensor J (SSJ) covering ions and electrons up to 30 keV to identify the plasma sheet precipitation boundaries and the Special Sensor Magnetometer (SSM) to infer currents. The three spacecraft have orbital planes separated in MLT that provide extensive coverage spanning the duskside over the course of this storm. Due to the much shorter orbital period of the low-Earth orbit spacecraft and the dense nature of magnetic field lines at high latitudes, the DMSP observations capture radial profiles of the inner magnetosphere between $L = 2$ and 6 in less than 10 min, and the three spacecraft pass through this L range four times per orbit. This allows the entire radial structure of the SAPS region to be sampled every 10–15 min at varying local times, contributing both broader- and higher-resolution spatial and temporal data to the equatorial picture from the Van Allen Probes, which require over 4 h to traverse from $L = 2$–6.

4. Van Allen Probes Observations and Interpretations

The following sections step through the duskside passes in which SAPS electric fields are observed by the Van Allen Probes during the 29 June 2013 storm. In Pass 1 (Figure 3), we show the basic structure of the particle boundaries and fields associated with SAPS. Pass 2 (Figure 4) contains a sharp electric field enhancement at the inner ion boundary, as well as evidence of multiple injections throughout the region. The lower energy ions (~20–40 keV) move earthward of the original ring current ions (~200–400 keV) in Pass 3 (Figure 5), and the final SAPS structure is observed in Pass 4 (Figure 6) before the end of the southward IMF period.

4.1. Pass 1: Van Allen Probe B

The first clear observation of the SAPS structure is shown in Figure 3 for an outbound pass from Van Allen Probe B (28 June 2013, 20–22 UT) near the beginning of the main phase of the storm. The IMF had been steadily southward for 2 h before this pass, and the spacecraft observes strong DC electric fields persisting for 40 min as the spacecraft moves from $L = 3.5$ to $L = 4.5$. We interpret this primarily as a spatial feature that the spacecraft passes through, because the general feature is present on multiple consecutive passes over many hours, although there are also temporal characteristics that will be addressed later. The spacecraft begins inside the plasmasphere, where density is large (Figure 3b), and then it crosses the plasmapause at the sharp gradient in density near 21:10 UT. We have defined the plasmapause as the most earthward location where the density drops below 50 cm^3, and this point is marked by a red square in Figure 3b.

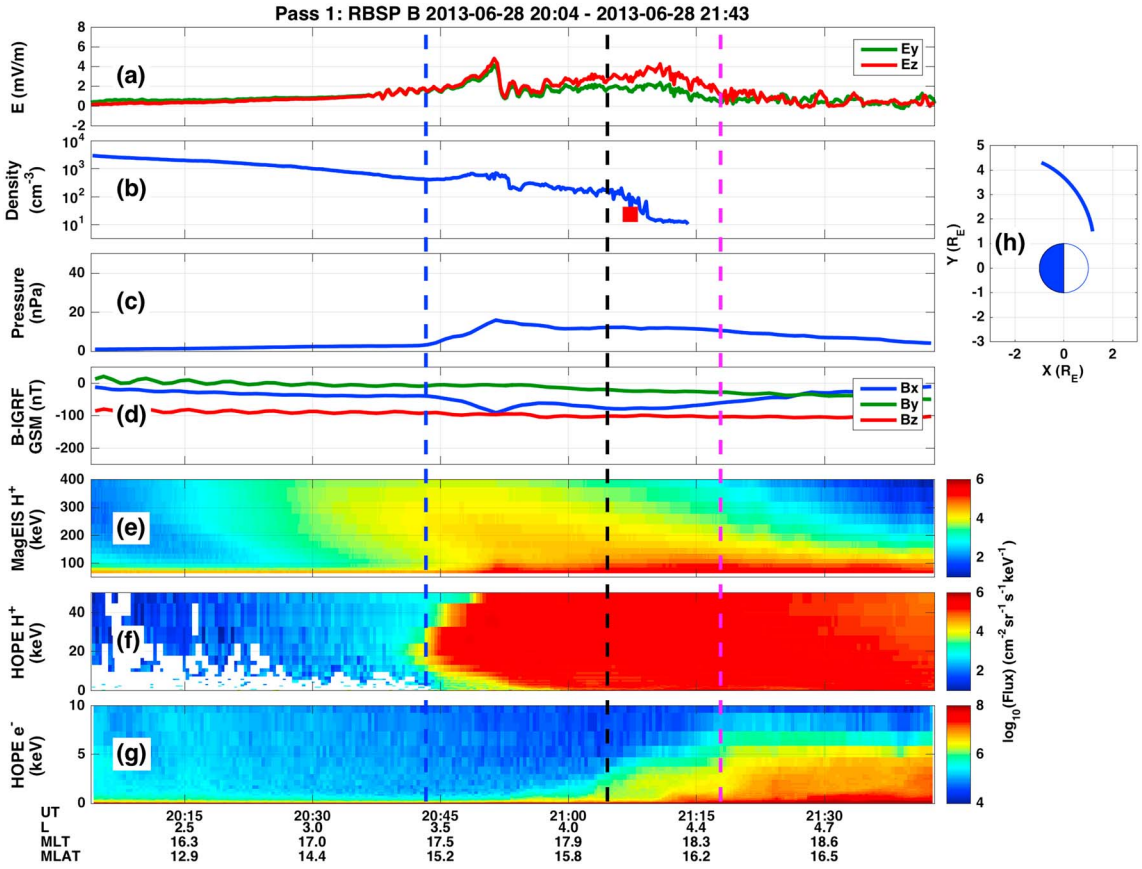

Figure 3. Example of SAPS from Van Allen Probe B on 28 June 2013. (a) DC electric field in the frame corotating with Earth from EFW, (b) density derived from spacecraft potential, (c) isotropic pressure computed from HOPE and MagEIS particle data, (d) EMFISIS magnetic field with IGRF removed, (e) differential proton fluxes between 50 and 400 keV from MagEIS, (f) differential proton fluxes between 1 and 50 keV from HOPE, (g) differential electron fluxes between 0 and 10 keV from HOPE, and (h) Van Allen Probe B orbit. The vertical lines show the inner boundaries for: 20 keV ions (blue), 2 keV electrons (black), and 5 keV electrons (magenta).

A high-energy (200–400 keV) ion population is encountered at $L = 3$ (Figure 3e), which was present before the storm and is part of the preexisting trapped ring current [e.g., *Daglis et al*., 1999; *Zhao et al*., 2015]. Next, a sharp lower energy (10–50 keV) ion boundary is encountered near $L = 3.5$ (Figure 3f, blue dashed line) that was not present on the previous pass. The ions form a "nose" configuration, where ~20 keV ions are encountered first, and higher and lower energy fluxes increase at larger radial distances. This is a spatial feature that is a consequence of the energy-dependent drift paths under the influence of corotation, convection, and magnetic gradient drifts [e.g., *Chen*, 1970; *Smith and Hoffman*, 1974].

There is an increase in pressure at the inner edge of the ions (Figure 3c, blue dashed line) that is accompanied by a negative perturbation in B_x GSM (Figure 3d). The blue dashed line indicates the innermost location where the 20 keV ion flux exceeds 10^4 ($cm^{-2}\,sr^{-1}\,s^{-1}\,keV^{-1}$). The pressure is calculated using ion and electron data with energies of 0.2 keV to 1 MeV from HOPE and MagEIS, assuming isotropic pitch angle distributions. *Zhao et al*. [2015] showed that the isotropic assumption has little effect on the magnitude of the computed pressure, and our focus is on the location of the pressure gradient rather than the absolute magnitude of the pressure. The magnetic field data shown are the measured magnetic field with the International Geomagnetic Reference Field (IGRF) removed, and slow variations are interpreted as indications of spatial gradients in the GSM Y direction. In the inner magnetosphere near the equatorial plane, the magnetic field is mostly oriented along GSM Z, so the parallel current can be written as

$$J_{\parallel} = \frac{1}{\mu_0}\left(\frac{\partial B_y}{\partial x} - \frac{\partial B_x}{\partial y}\right)$$

The negative B_x perturbation as the spacecraft moves in Y is an indication of a field-aligned current from the equatorial magnetosphere to the ionosphere in the Northern Hemisphere, which is expected given the

observed pressure gradient at the inner edge of the ions. Had the spacecraft been off-equator in the Southern Hemisphere rather than in the Northern Hemisphere, we would expect a positive B_x perturbation corresponding to a field-aligned current directed toward the ionosphere in the south. Similarly, a positive B_x perturbation in the Northern Hemisphere is an indication of a field-aligned current out of the ionosphere.

At $L = 4.1$, more than 0.5 R_E after measuring the nose ion population, the spacecraft meets the inner edge of the 2 keV electrons (Figure 3g, black dashed line), and the inner boundary for 5 keV electrons is observed at $L = 4.6$ (Figure 3g, magenta dashed line). The black and magenta dashed lines indicate the innermost location where the 2 and 5 keV electron fluxes exceed 10^6 ($cm^{-2}\,sr^{-1}\,s^{-1}\,keV^{-1}$), respectively. The outer edge of the enhanced electric field region corresponds well with the inner boundary of the 5 keV electrons, but not with the 2 keV electrons. It is possible that the auroral precipitation boundary associated with the outer edge of the SAPS region maps more closely to the 5 keV equatorial boundary, rather than the 2 keV boundary.

The electrons display a different energy dispersion than the ions, where lower energy electrons are observed before higher-energy electrons. The electron enhancement above 2 keV is also mostly located outside of the plasmasphere, whereas the ion enhancement penetrates inside the plasmasphere. The electron energy is mostly below 5 keV, while the ion flux enhancement extends from 10 to 50 keV. The difference in energy may be attributed to the characteristic energy of the plasma sheet ions being approximately a factor of 7 higher than plasma sheet electrons [*Baumjohann et al.*, 1989], as well as the fact that the ions drift closer to Earth at dusk and therefore gain more energy through conservation of the first adiabatic invariant than the electrons.

The pressure gradient near the sharp inner edge of the plasma sheet ions leads to field-aligned currents that flow into the ionosphere, and the inner edge of the plasma sheet electrons is related to the electron precipitation boundary in the ionosphere, which has an associated field-aligned current out of the ionosphere. In the postdusk sector, precipitating electrons are the primary driver of ionospheric conductivity [e.g., *Burke et al.*, 1998]. Because the ions are earthward of the electrons in the equatorial magnetosphere, the field-aligned current maps into the ionosphere at a lower latitude than the electron precipitation boundary, and the current closes horizontally poleward via the Pedersen current though a region of low conductivity in the ionosphere [e.g., *Yeh et al.*, 1991]. The finite conductivity and poleward current cause a large poleward electric field and corresponding fast westward flow. This high-latitude electric field maps to the equatorial magnetosphere as a radially outward electric field, which is consistent with the broad enhancement in the GSM Y electric field observed by the Van Allen Probes near dusk between the inner edges of the plasma sheet ions and electrons. Qualitatively, the enhanced electric fields in Figure 3 agree with the theoretical description of SAPS, although there is some ambiguity in defining the electron precipitation boundary based on the equatorial magnetospheric particle data.

4.2. Pass 2: Van Allen Probe A

The radial profile of the particles, pressure, field-aligned currents, and electric fields are shown for the following outbound pass by Van Allen Probe A in Figure 4. These observations occur 4 h after the previous example, and the IMF has been steadily southward for 8 h. Again, the spacecraft encounters a high-energy (200–400 keV) ion population in nearly the same location as the previous pass, followed by a lower energy ion population with a nose energy near 30 keV. The lower energy population has a similar spatial structure to the one previously observed by Van Allen Probe B, except that it has moved earthward from $L = 3.5$ to $L = 3.0$, and the nose energy has increased from 20 to 30 keV.

On the previous pass, there was a strong pressure gradient and field-aligned current located at the inner edge of the nose ions, but in this case the pressure gradient is smaller and the field-aligned current is either small or nonexistent based on the magnetic field data (Figure 4d, blue dashed line). Despite the lack of a strong pressure gradient, there is an elevated electric field of ~2 mV/m between $L = 2.2$ and 3.6, which is large relative to statistical averages at these low L shells, although not uncommon during very active times. Data from CRRES and THEMIS (Time History of Events and Macroscale Interactions during Substorms) show that the average dawn-dusk electric field tends to be less than 0.6 mV/m and decreasing in magnitude below $L = 3.5$ during moderate storms ($3 < \underline{Kp} < 6$). However, during the largest storms ($Kp > 6$) there can be an increasing trend extending inside $L = 3$ with average magnitudes greater than 1.5 mV/m [*Rowland and Wygant*, 1998; *Califf et al.*, 2014].

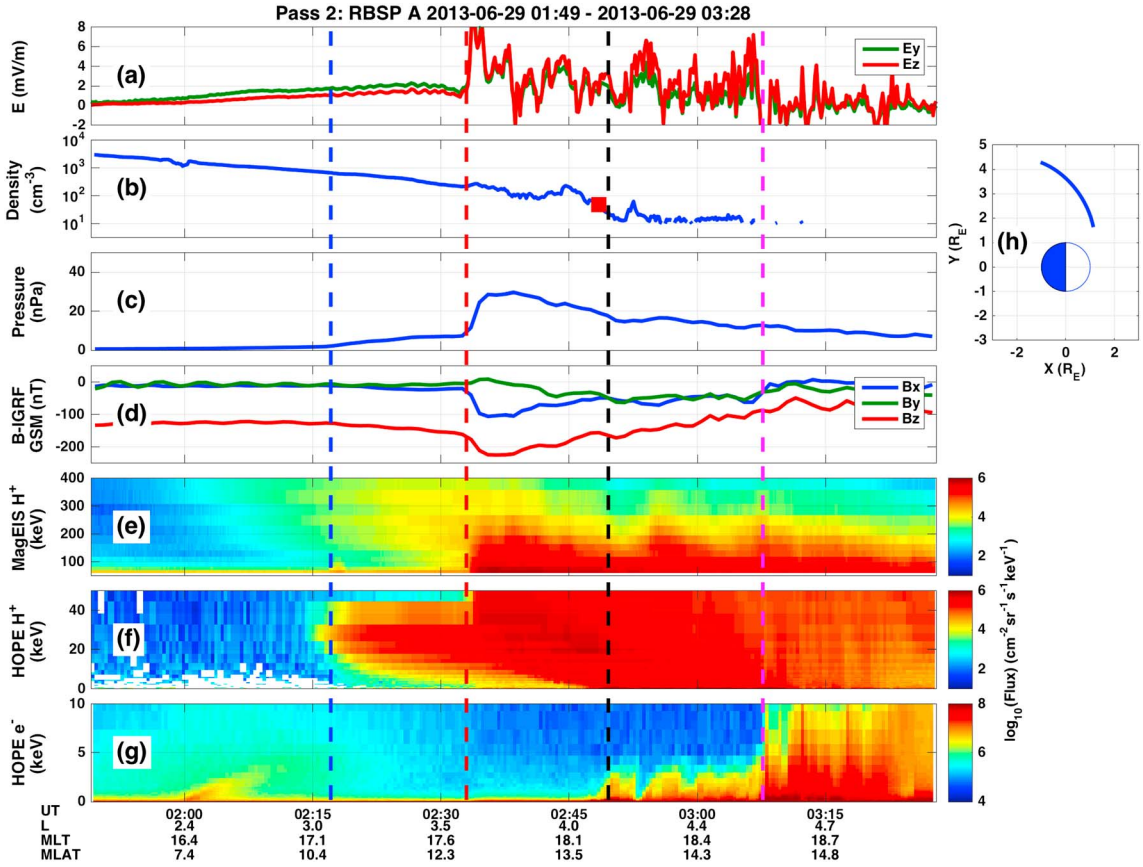

Figure 4. Example of SAPS from Van Allen Probe A on 29 June 2013 in the same format as Figure 3. The vertical lines show the inner boundaries for 20 keV ions (blue), 80 keV ions (red), 2 keV electrons (black), and 5 keV electrons (magenta).

This low-L electric field enhancement is not clearly related to plasma sheet particle boundaries as it begins 0.8 R_E earthward of the inner edge of the nose ions. This is an example of the high-latitude convection electric field penetrating directly to low latitudes. Penetration electric fields are typically described as short-duration events related to rapid changes in the polar cap potential on timescales faster than the time required to establish ring current shielding [e.g., *Greenspan et al.*, 1991; *Burke et al.*, 1998]. However, observations [*Mannucci et al.*, 2008] and Rice Convection Model (RCM) simulations [e.g., *Garner et al.*, 2004] have shown that penetration electric fields can last for hours during large storms.

A second, more dramatic pressure gradient is encountered at $L = 3.6$ that is accompanied by a very large ~10 mV/m spike in the electric field (red dashed line) and clear magnetic perturbations in both B_x and B_z. At the red dashed line, the 80 keV ion flux increased by more than a factor of 2 within 0.1L. This electric field spike is followed by a fluctuating electric field with a net positive GSM Y DC component that persists until the spacecraft encounters the inner edge of the 5 keV plasma sheet electrons at $L = 4.5$ (magenta dashed line). The electric field does decrease briefly at the 2 keV electron boundary (black dashed line). We consider the broad region between the ion and electron boundaries (red and magenta dashed lines) to be the SAPS region. The initial electric field spike is an example of a subauroral ion drift (SAID), which is a more narrow and intense feature within the SAPS region that is generally understood to arise through the same magnetosphere-ionosphere coupling mechanism as SAPS [e.g., *Anderson et al.*, 2001]. The large electric field at $L = 3.6$ is clearly inside the plasmapause, and it is correlated with the pressure increase related to a dramatic flux enhancement for ions between 20 and 200 keV (Figures 4e and 4f).

4.3. Pass 3: Van Allen Probe B

The next pass in Figure 5 occurs 4 h later, and the low-energy (20–40 keV) ion nose population has moved farther earthward, while the inner boundary of the high-energy ion population has remained relatively

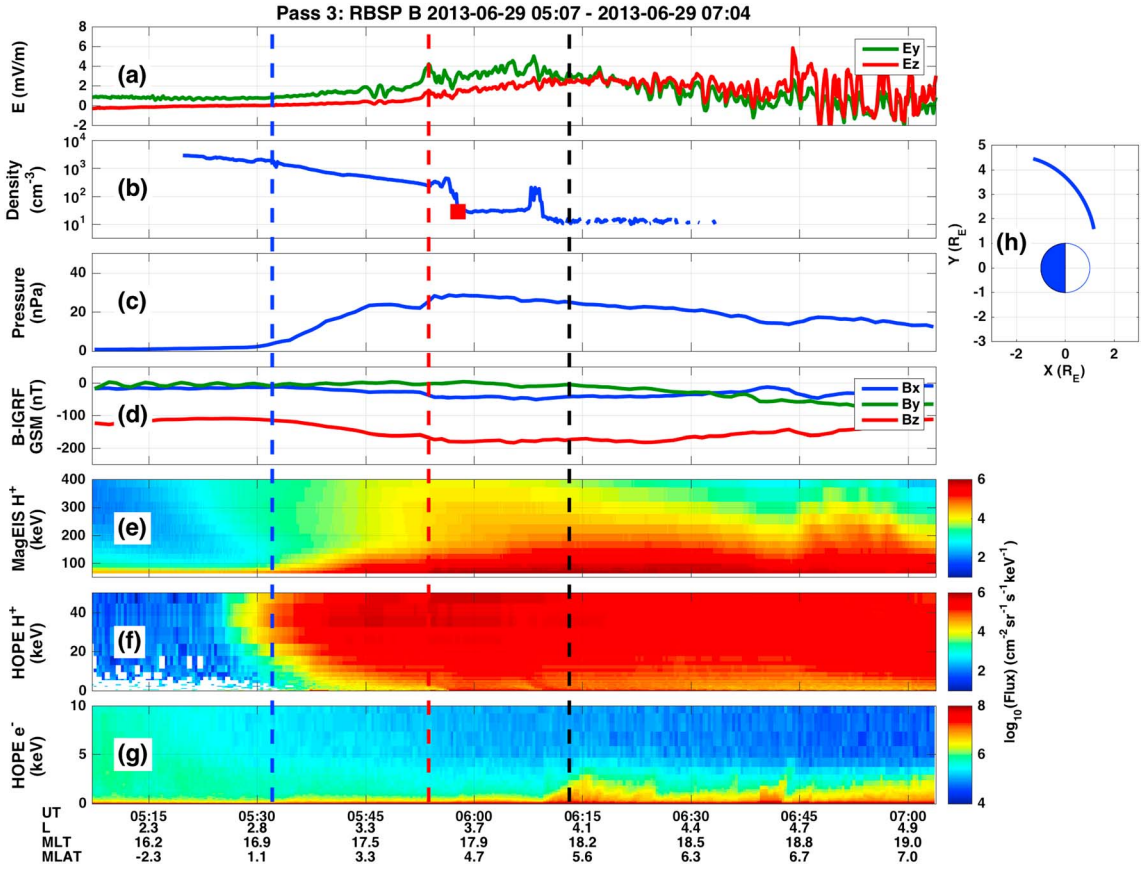

Figure 5. Example of SAPS from Van Allen Probe B on 29 June 2013 in the same format as Figure 3. The vertical lines show the inner boundaries for 20 keV ions (blue), 80 keV ions (red), and 2 keV electrons (black).

constant during the storm. This pass occurs 12 h into the steady southward IMF period of the storm, and the recovery phase has yet to begin. Similar to the previous pass, there is evidence that the electric field penetrates earthward of the inner edge of the plasma sheet ions and associated pressure gradient with a magnitude of ~1 mV/m extending below $L = 2.1$. As was described previously, this is an example of a long-lasting penetration electric field [e.g., *Mannucci et al.*, 2008; *Garner et al.*, 2004] and is not caused by SAPS.

At the inner edge of the lower energy nose ion population (blue dashed line) there is a gradual increase in the electric field, and then a sharp enhancement occurs coincident with the inner boundary of the higher-energy ions that is consistent with a SAPS electric field (red dashed line). There is a flux increase of nearly a factor of 2 for 80 keV ions at the red dashed line. Our interpretation is that an additional injection of 10s keV ions (Figure 5e) happened to coincide with the preexisting high-energy ions (200–400 keV), causing an increased pressure gradient, field-aligned current, and increased magnetospheric electric field, rather than the electric field being caused by the high-energy ions directly, as this population has been steady throughout the storm. In the region between the initial nose ions and the new injection, the pressure has increased by a factor of 2–3 relative to the previous pass (Figures 4 and 5, blue and red dashed lines), but the electric field is slightly smaller in magnitude. This demonstrates the significance of pressure gradients, rather than absolute pressure magnitude, in driving field-aligned currents and modifying the magnetospheric electric field.

The SAPS electric field in this case appears to extend from the inner edge of the 20 keV ions at $L = 2.8$ (Figure 5, blue dashed line) out to $L = 4.5$. However, the electron boundary that defines the outer edge of the classical SAPS region is not so clear. In the first two passes, there was a sharp increase in flux of electrons up to at least 5 keV near $L = 4.5$ that corresponded well with the outer boundary of the enhanced electric field region, but in this pass the electron energy is mostly below 2 keV.

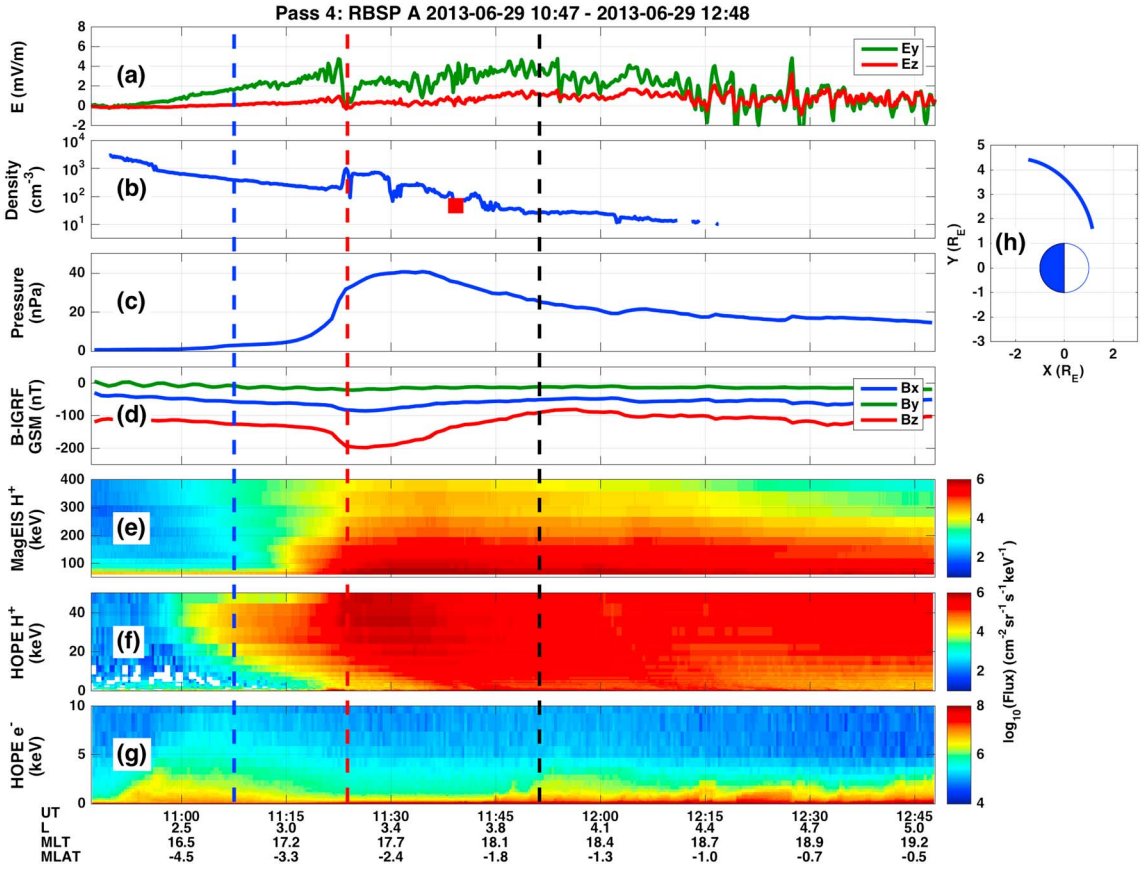

Figure 6. Example of SAPS from Van Allen Probe A on 29 June 2013 in the same format as Figure 3. The vertical lines show the inner boundaries for 20 keV ions (blue), 80 keV ions (red), and 2 keV electrons (black).

4.4. Pass 4: Van Allen Probe A

The final Van Allen Probe pass that clearly observes the SAPS boundaries and electric field signatures is shown in Figure 6. This example occurs at the end of the steady southward IMF period just before the recovery phase of the storm. In this case, the nose ion population has moved farther inward to $L = 2.5$ and the nose energy is now greater than 40 keV, rather than ~20 keV as in the first pass. The factor of 2 increase in energy is consistent with the expected energy gain due to adiabatic transport from $L = 3.5$ to $L = 2.5$. The high-energy population (200–400 keV) has remained roughly in the same location as in the initial pass. There is an increase in the electric field beginning at the inner edge of the lower energy ions, and an additional enhancement just inside the inner edge of the higher-energy ions, similar to the previous pass. The 1–2 mV/m penetration electric field at low L shells inside of the inner edge of the nose ions is not present in this case.

At the large pressure gradient (red dashed line), there is a rapid decrease in the electric field, followed by a gradual broad enhancement extending out to $L = 4.4$. Similar to the previous case, the inner edge of the plasma sheet electrons is difficult to identify, and the electron energy is mostly below 2 keV. One difference between the first two passes in which >5 keV electrons were observed near the outer electric field boundary and the last two passes where electron energy was lower is the magnetic latitude of the spacecraft. The higher-energy electrons were observed at MLAT > 15°, but the last two passes were closer to the magnetic equator (MLAT < 7°) and did not observe the >5 keV electrons. It is possible that the difference is related to magnetic mapping errors, where the actual magnetic field for the first two passes maps to larger equatorial radial distances than the dipole model used to approximate the L shell.

4.5. Van Allen Probes and DMSP

In Figure 7, the Van Allen Probe A outbound pass (Pass 2, Figure 4) is compared to two DMSP passes by F17 and F18 traversing through the dusk sector at high latitudes. The data are plotted versus L shell to compare

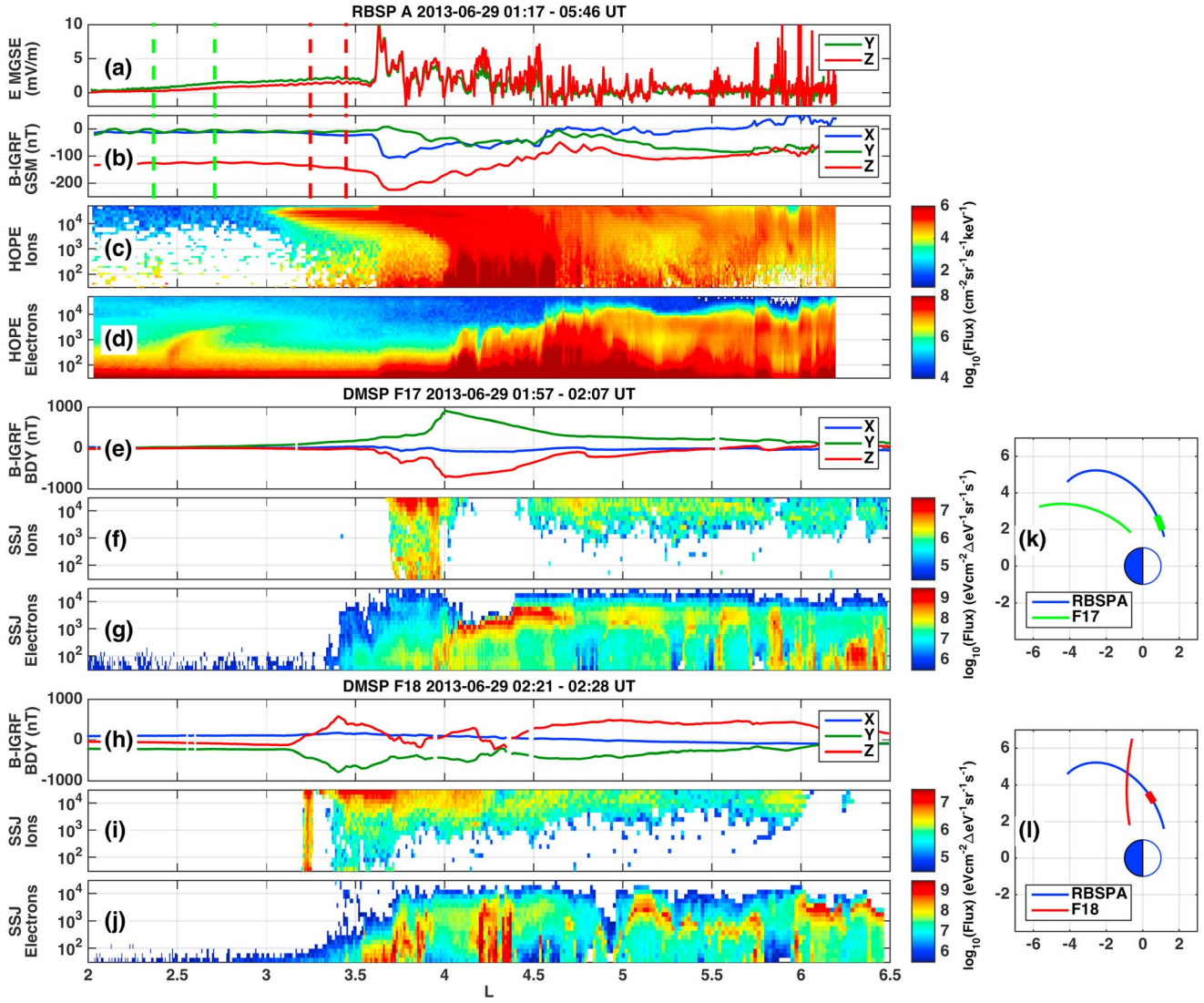

Figure 7. Spatial profiles of the electric field, magnetic perturbations, and particle fluxes from the Van Allen Probes and DMSP near a large electric field spike in the inner magnetosphere. The top panels show RBSP A (a) EFW electric field, (b) EMFISIS magnetic field with IGRF removed, (c) HOPE ion fluxes, and (d) HOPE electron fluxes for one outbound duskside pass. Below are DMSP F17 (e) SSM magnetic field with IGRF removed, (f) SSJ ion fluxes, and (g) SSJ electron fluxes. (h–j) A separate DMSP F18 pass in the same format as Figures 7e–7g. All data are plotted against L shell, although the Van Allen Probes sample the spatial region over 4.5 h while the DMSP passes occur in 7–10 min. The orbit plots in Figures 7k and 7l show (L, MLT) coordinates projected into the equatorial plane, and the location of RBSP A during each DMSP pass is highlighted in the orbit plots in Figures 7k and 7l, and also with the vertical dashed lines in Figures 7a and 7b using the same color scheme to identify DMSP F17 and F18.

the spatial structure of the equatorial and high-latitude magnetic perturbations and particle boundaries. The Van Allen Probe L shell is calculated using an Earth-centered dipole model, and the DMSP L shell is based on altitude adjusted corrected geomagnetic coordinates. Our goal is to qualitatively examine the relative spatial positions of features related to SAPS.

It is important to note that the Van Allen Probes are in geotransfer orbits near the equatorial plane, and the spacecraft require 4.5 h to traverse from $L = 2–6$, while the DMSP spacecraft are in ~800 km Sun-synchronous polar orbits with orbital periods of ~90 min, enabling them to sample the high-latitude magnetic field footpoints corresponding to $L = 2–6$ in ~10 min. Therefore, the DMSP data provide a faster snapshot of the radial profile of the particle and field structures, while the Van Allen Probe data capture both long-lasting, large-scale spatial features, as well as temporal features on timescales much shorter than the 4.5 h required to sample the entire spatial profile.

The Van Allen Probe A data show an unusually large electric field of ~10 mV/m at $L = 3.6$ (Figure 7a), and the DMSP F17 (Figures 7e–7g) and F18 (Figures 7h–7j) passes occur 30 and 6 min before the spike is observed in the equatorial plane, respectively. The relative magnetic tracks of Van Allen Probe A, DMSP F17, and DMSP F18 are shown in Figures 7k and 7l, where the L and MLT coordinates have been plotted in the equatorial plane. The location of Van Allen Probe A during each DMSP pass is indicated by color-coded vertical dashed lines in Figure 7a. For example, the red vertical dashed lines indicate the location of Van Allen Probe A over the course of the DMSP F18 pass from $L = 2$–6 plotted in Figures 7h–7j.

The magnetic field data from DMSP are shown with the IGRF subtracted out, and a slope in B_z, which is aligned with the orbit normal vector, is interpreted as a spatial gradient indicating a field-aligned current. The sign of the B_z perturbation relative to the direction of field-aligned current is opposite between the F17 and F18 data in this case, because the spacecraft are in different hemispheres, with F17 being in the south and F18 in the north. In each of the DMSP passes, the spacecraft first encounters a sharp ion precipitation boundary with tens of keV energy followed by a dispersed electron precipitation boundary. The ion boundary is accompanied by a field-aligned current into the ionosphere, marked by the slope in B_z in Figures 7e and 7h, and a current out of the ionosphere with an opposite B_z perturbation is measured with the electron precipitation boundary. These high-latitude particle boundaries and associated field-aligned currents correspond well with the features measured by Van Allen Probe A in the equatorial plane, despite the uncertainties involved in magnetic mapping.

An interesting feature in the DMSP data is the existence of multiple alternating field-aligned current structures between $L = 3$ and 5. With each change in slope of B_z, there are alternating regions of ion and electron precipitation. To this point in the paper, the SAPS region has been discussed in terms of a steady spatial separation between the plasma sheet ions and electrons; however, these data suggest that the region is composed of multiple layers of particle boundaries and alternating current structures. The Van Allen Probe A magnetic field data also support this view: there are multiple variations in the slope of B_x (Figure 7b) between $L = 3.5$ and 5 that are correlated with fluctuations in the electric field and particle pressure. These alternating current structures may be a series of incoming discrete injections from the tail related to the elevated substorm activity during this period (Figure 3e).

If we assume the DMSP data provide a snapshot of the spatial separation between successive injection fronts, and the Van Allen Probes data measure the injections passing over the relatively stationary spacecraft, we can estimate the propagation speed of the injection structures. The magnetic perturbations from DMSP are separated by approximately 1 R_E when mapped to the equatorial plane and between $L = 3.5$ and 5 Van Allen Probe A measures magnetic field fluctuations with a period of ~2–4 min. This results in an earthward propagation speed of 25–50 km/s. *Reeves et al*. [1996] used dispersionless electron injection signatures from LANL and CRRES to estimate the radial propagation of the injections from $L = 6.6$ (geosynchronous orbit) to $L = 5$ and found an average earthward propagation speed of 24 km/s, which is consistent with our estimate.

The injections are initiated farther back in the tail, where magnetic reconnection launches a dipolarization front earthward with speeds of 200–500 km/s between 10 and 20 R_E [*Runov et al*., 2011]. Most dipolarization fronts slow down and stop at geosynchronous orbit or beyond [e.g., *Sergeev et al*., 2012], and they are not expected to penetrate inside the plasmasphere. The much slower propagation speeds from our study and *Reeves et al*. [1996] are consistent with earthward injections that are slowing down in the inner magnetosphere. By connecting the magnetic perturbations between the Van Allen Probes and DMSP, we suggest that the electric field pulse at $L = 3.6$, which is inside the plasmasphere, is the remnant of a dipolarization front, where the initial dipolarization in the magnetic field farther back in the tail evolves into a SAPS/SAID structure in the inner magnetosphere.

In addition to the radial spatial structure of the SAPS region revealed within a single DMSP pass (~10 min), the three DMSP spacecraft also show variation in the particle precipitation boundaries and field-aligned currents between successive passes close together in time and MLT. The data are consistent with a picture of multiple, narrow in MLT injections occurring on timescales of minutes, and the integrated effect producing a buildup of pressure, field-aligned currents, and the broad region of strong electric fields in the equatorial region. Recent studies have suggested that small-scale injections may be of equal or greater importance than large-scale convection in transporting plasma sheet particles into the inner magnetosphere-based Van Allen Probes observations [*Gkioulidou et al*., 2014] as well as RCM-E simulations [*Yang et al*., 2015], and our observations support this view.

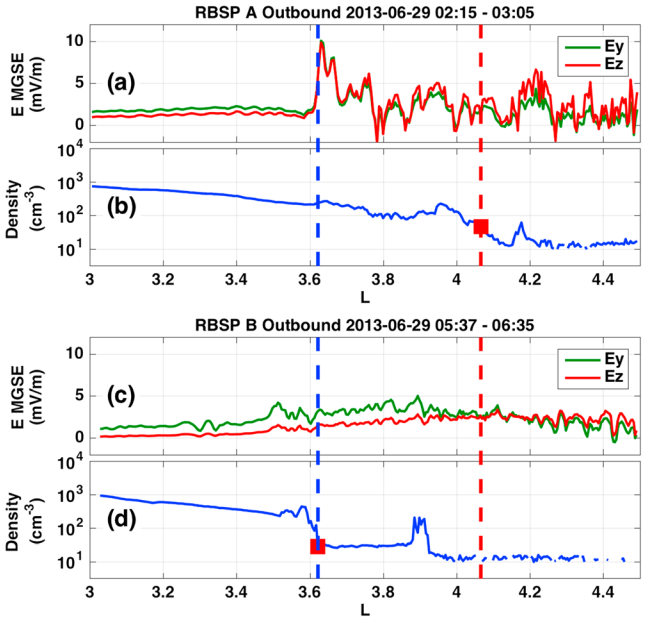

Figure 8. Consecutive outbound duskside passes from Van Allen Probes A and B showing strong electric fields and a subsequent inward motion of the plasmapause.

5. SAPS Impact

5.1. Plasmasphere Erosion

As was seen from the Van Allen Probes particle and electric field data (Figures 3–6), the inner edge of the plasma sheet ions penetrates inside the outer edge of the plasmapause at dusk, and the SAPS electric field can be enhanced partially inside the plasmasphere. Two consecutive Van Allen Probes duskside passes are shown in Figure 8, and the effect of the large electric fields inside the plasmasphere is apparent. We define the plasmapause as the most earthward location where the density drops below 50 cm^3. In Figure 9a, Van Allen Probe A observes a ~10 mV/m spike near $L = 3.6$ that was associated with a strong pressure gradient and a magnetic perturbation, and the plasmapause is located at $L = 4.1$ based on the gradient in spacecraft potential. Four hours later, Van Allen Probe B passes through the same spatial region, and the plasmapause has moved inward to the location of the previously observed large electric field spike.

This is a direct example of the effect of the plasma sheet ions drifting through the outer edge of the plasmasphere, causing a large electric field that convects away the lower energy particles and redefines the plasmapause at a lower L value. While plasmasphere erosion and the formation of plumes have historically been explained by variations in the strength of the convection electric field, this example shows a clear correlation between localized electric fields on the duskside and changes in the plasmapause, adding further evidence that SAPS should not be ignored in basic descriptions of magnetospheric electric fields and plasmasphere dynamics [e.g., *Goldstein et al.*, 2003]. The connection between SAPS and plasmasphere erosion is important due to the impact the plasmasphere has on the coupled magnetospheric system, including the propagation of waves that affect the loss and energization of radiation belt electrons.

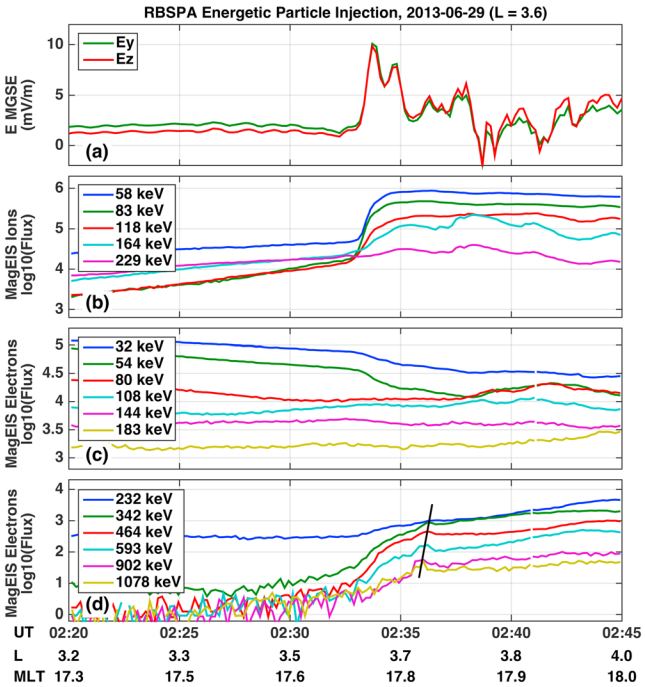

Figure 9. A large-amplitude electric field spike from EFW on (a) Van Allen Probes A with corresponding (b) ion and (c–d) electron fluxes from MagEIS. The black line in Figure 9d shows a dispersed electron injection signature.

5.2. Particle Energization

The same electric field spike that was related to plasmapause motion in the previous section is also correlated with flux enhancements in the

higher-energy ion and electron populations. Figure 9 shows the electric field along with ion and electron fluxes for selected energies from MagEIS. Across the ~10 mV/m electric field spike, the ions display flux increases of 1–2 orders of magnitude between 30 keV (not shown) and 170 keV (Figure 9b). Shortly after the large electric field is observed, there is an enhancement in 200 keV to 1 MeV electron flux and a decrease in 50–80 keV flux. A detailed analysis of the relationship between the electric field pulse and the energetic particle response is outside of the scope of this paper, but the correlation between SAPS and 100s keV electrons is interesting and will be the subject of a future study.

6. Summary

This study shows observations of the particles and fields associated with SAPS during an extended period of southward IMF during the 29 June 2013 geomagnetic storm. Overall, the major aspects of the traditional SAPS description were observed in relation to the strong electric fields measured by the Van Allen Probes. Near dusk, plasma sheet ions contributed to increased pressure in the inner magnetosphere, causing field-aligned currents to flow into the ionosphere. The plasma sheet electron boundary was observed to be radially outward from the ion boundary both at the equatorial plane and at high latitudes, and consequently, the keV electron precipitation boundary in the ionosphere was located at a higher latitude than the field-aligned current associated with the ions. This spatial arrangement led to a current closing through a low-conductivity region, resulting in a strong electric field that mapped back to the equatorial magnetosphere.

Although most of the observations were in agreement with the traditional SAPS picture, there were cases of enhanced electric fields earthward of the inner edge of the plasma sheet ions ($L < 2.5$) that are examples of long-duration penetration electric fields. Also, the ion inner edge was consistently identified in the Van Allen Probes data and was observed to move earthward throughout the storm, but the equatorial plasma sheet electron boundary was not as clear in two of the four passes. The outer boundary of the SAPS region corresponded to the inner boundary of 5 keV electrons in the first two passes; however, the 5 keV electron boundary was not observed in the last two passes. We suspect that the difference may be related to magnetic mapping.

The combination of the equatorial Van Allen Probes and high-latitude DMSP spacecraft showed that the SAPS region can be characterized as a broad spatial region persisting for hours that also contains significant small-scale spatial and temporal variation within. We interpret multiple variations in the magnetic field data as earthward propagating spatial structures separated by ~1 R_E in the equatorial plane with speeds between 25 and 50 km/s. These features may be the earthward extent of substorm-related dipolarization fronts slowing down and piling up in the inner magnetosphere, resulting in the integrated effect of a large pressure gradient at the inner edge of the plasma sheet ions. We also showed that a SAPS does penetrate inside the plasmasphere and that there may be a relationship between SAPS electric fields and 100s keV electron enhancements at low L shells in the inner magnetosphere.

Acknowledgments

The work at the University of Colorado was supported in part by NASA/Van Allen Probes ECT and EFW funding through JHU/APL contract 967399 under prime NASA contract NAS5-01072, NASA/THEMIS project NAS5-02099, and NASA Earth and Space Sciences Fellowship (NESSF) award NNX15AT57H. The work at Rice was supported by NASA HGC grant NNX14AN55G. Van Allen Probes data are available on the ECT, EFW, and EMFISIS websites, and OMNI and DMSP data can be found at http://cdaweb.gsfc.nasa.gov.

References

Anderson, P. C., D. L. Carpenter, K. Tsuruda, T. Mukai, and F. J. Rich (2001), Multisatellite observations of rapid subauroral ion drifts (SAID), *J. Geophys. Res.*, *106*, 29,585–29,600, doi:10.1029/2001JA000128.

Banks, P. M., and F. Yasuhara (1978), Electric fields and conductivity in the nighttime *E*-region: A new magnetosphere-ionosphere-atmosphere coupling effect, *Geophys. Res. Lett.*, *5*, 1047–1050, doi:10.1029/GL005i012p01047.

Baumjohann, W., G. Paschmann, and C. A. Cattell (1989), Average plasma properties in the central plasma sheet, *J. Geophys. Res.*, *94*, 6597–6606, doi:10.1029/JA094iA06p06597.

Blake, J. B., et al. (2013), The Magnetic Electron Ion Spectrometer (MagEIS) instruments aboard the Radiation Belt Storm Probes (RBSP) spacecraft, *Space Sci. Rev.*, *179*, 383–421, doi:10.1007/s11214-013-9991-8.

Burke, W. J., N. C. Maynard, M. P. Hagan, R. A. Wolf, G. R. Wilson, L. C. Gentile, M. S. Gussenhoven, C. Y. Huang, T. W. Garner, and F. J. Rich (1998), Electrodynamics of the inner magnetosphere observed in the dusk sector by CRRES and DMSP during the magnetic storm of June 4–6, 1991, *J. Geophys. Res.*, *103*, 29,399–29,418, doi:10.1029/98JA02197.

Burke, W. J., A. G. Rubin, N. C. Maynard, L. C. Gentile, P. J. Sultan, F. J. Rich, O. de La Beaujardière, C. Y. Huang, and G. R. Wilson (2000), Ionospheric disturbances observed by DMSP at middle to low latitudes during the magnetic storm of June 4–6, 1991, *J. Geophys. Res.*, *105*, 18,391–18,405, doi:10.1029/1999JA000188.

Califf, S., et al. (2014), THEMIS measurements of quasi-static electric fields in the inner magnetosphere, *J. Geophys. Res. Space Physics*, *119*, 9939–9951, doi:10.1002/2014JA020360.

Chen, A. J. (1970), Penetration of low-energy electrons deep into the magnetosphere, *J. Geophys. Res.*, *75*, 2458–2467, doi:10.1029/JA075i013p02458.

Daglis, I. A., R. M. Thorne, W. Baumjohann, and S. Orsini (1999), The terrestrial ring current: Origin, formation, and decay, *Rev. Geophys.*, *37*, 407–438, doi:10.1029/1999RG900009.

Foster, J. C., and W. J. Burke (2002), SAPS: A new categorization for subauroral electric fields, *Eos Trans. AGU*, *83*, 393–394, doi:10.1029/2002EO000289.

Foster, J. C., and H. B. Vo (2002), Average characteristics and activity dependence of the subauroral polarization stream, *J. Geophys. Res.*, *107*(A12), 1475, doi:10.1029/2002JA009409.

Funsten, H., et al. (2013), Helium, Oxygen, Proton, and Electron (HOPE) mass spectrometer for the radiation belt storm probes mission, *Space Sci. Rev.*, *179*, 1–62, doi:10.1007/s11214-013-9968-7.

Garner, T. W., R. A. Wolf, R. W. Spiro, W. J. Burke, B. G. Fejer, S. Sazykin, J. L. Roeder, and M. R. Hairston (2004), Magnetospheric electric fields and plasma sheet injection to low L-shells during the 4–5 June 1991 magnetic storm: Comparison between the Rice Convection Model and observations, *J. Geophys. Res.*, *109*, A02214, doi:10.1029/2003JA010208.

Gkioulidou, M., A. Y. Ukhorskiy, D. G. Mitchell, T. Sotirelis, B. H. Mauk, and L. J. Lanzerotti (2014), The role of small-scale ion injections in the buildup of Earth's ring current pressure: Van Allen Probes observations of the 17 March 2013 storm, *J. Geophys. Res. Space Physics*, *119*, 7327–7342, doi:10.1002/2014JA020096.

Goldstein, J., B. R. Sandel, M. R. Hairston, and P. H. Reiff (2003), Control of plasmaspheric dynamics by both convection and sub-auroral polarization stream, *Geophys. Res. Lett.*, *30*(24), 2243, doi:10.1029/2003GL018390.

Greenspan, M. E., C. E. Rasmussen, W. J. Burke, and M. A. Abdu (1991), Equatorial density depletions observed at 840 km during the Great Magnetic Storm of March 1989, *J. Geophys. Res.*, *96*(A8), 13,931–13,942, doi:10.1029/91JA01264.

Kataoka, R., D. Shiota, E. Kilpua, and K. Keika (2015), Pileup accident hypothesis of magnetic storm on 17 March 2015, *Geophys. Res. Lett.*, *42*, 5155–5161, doi:10.1002/2015GL064816.

Kletzing, C. A., et al. (2013), The Electric and Magnetic Field Instrument and Suite and Integrated Science (EMFISIS) on RBSP, *Space Sci. Rev.*, *179*, 127–181, doi:10.1007/s11214-013-9993-6.

Korth, H., M. F. Thomsen, J. E. Borovsky, and D. J. McComas (1999), Plasma sheet access to geosynchronous orbit, *J. Geophys. Res.*, *104*, 25,047–25,061, doi:10.1029/1999JA900292.

Kurth, W. S., S. De Pascuale, J. B. Faden, C. A. Kletzing, G. B. Hospodarsky, S. Thaller, and J. R. Wygant (2015), Electron densities inferred from plasma wave spectra obtained by the waves instrument on Van Allen Probes, *J. Geophys. Res. Space Physics*, *120*, 904–914, doi:10.1002/2014JA020857.

Mannucci, A. J., B. T. Tsurutani, M. A. Abdu, W. D. Gonzalez, A. Komjathy, E. Echer, B. A. Iijima, G. Crowley, and D. Anderson (2008), Superposed epoch analysis of the dayside ionospheric response to four intense geomagnetic storms, *J. Geophys. Res.*, *113*, A00A02, doi:10.1029/2007JA012732.

Puhl-Quinn, P. A., H. Matsui, E. Mishin, C. Mouikis, L. Kistler, Y. Khotyaintsev, P. M. E. Décréau, and E. Lucek (2007), Cluster and DMSP observations of SAID electric fields, *J. Geophys. Res.*, *112*, A05219, doi:10.1029/2006JA012065.

Reeves, G. D., R. W. H. Friedel, M. G. Henderson, A. Korth, P. S. McLachlan, and R. D. Belian (1996), Radial propagation of substorm injections, in *International Conference on Substorms-3*, *Spec. Publ. ESA SP-339*, 579 pp., Eur. Space Agency, Paris.

Rowland, D. E., and J. R. Wygant (1998), Dependence of the large-scale, inner magnetospheric electric field on geomagnetic activity, *J. Geophys. Res.*, *103*, 14,959–14,964, doi:10.1029/97JA03524.

Runov, A., V. Angelopoulos, X. -Z. Zhou, X. -J. Zhang, S. Li, F. Plaschke, and J. Bonnell (2011), A THEMIS multicase study of dipolarization fronts in the magnetotail plasma sheet, *J. Geophys. Res.*, *116*, A05216, doi:10.1029/2010JA016316.

Saikin, A. A., J. C. Zhang, R. C. Allen, C. W. Smith, L. M. Kistler, H. E. Spence, R. B. Torbert, C. A. Kletzing, and V. K. Jordanova (2015), The occurrence and wave properties of H + -, He + -, and O + -band EMIC waves observed by the Van Allen Probes, *J. Geophys. Res. Space Physics*, *120*, 7477–7492, doi:10.1002/2015JA021358.

Schunk, R. W., P. M. Banks, and W. J. Raitt (1976), Effects of electric fields and other processes upon the nighttime high-latitude *F* layer, *J. Geophys. Res.*, *81*, 3271–3282, doi:10.1029/JA081i019p03271.

Sergeev, V. A., I. A. Chernyaev, S. V. Dubyagin, Y. Miyashita, V. Angelopoulos, P. D. Boakes, R. Nakamura, and M. G. Henderson (2012), Energetic particle injections to geostationary orbit: Relationship to flow bursts and magnetospheric state, *J. Geophys. Res.*, *117*, A10207, doi:10.1029/2012JA017773.

Smith, P., and R. A. Hoffman (1974), Direct observations in the dusk hours of the characteristics of the storm time ring current particles during the beginning of magnetic storms, *J. Geophys. Res.*, *79*, 966–971, doi:10.1029/JA079i007p00966.

Southwood, D. J., and R. A. Wolf (1978), An assessment of the role of precipitation in magnetospheric convection, *J. Geophys. Res.*, *83*, 5227–5232, doi:10.1029/JA083iA11p05227.

Wygant, J., et al. (2013), The electric field and waves instruments on the radiation belt storm probes mission, *Space Sci. Rev.*, *179*(1–4), 183–220, doi:10.1007/s11214-013-0013-7.

Yang, J., F. R. Toffoletto, R. A. Wolf, and S. Sazykin (2015), On the contribution of plasma sheet bubbles to the storm time ring current, *J. Geophys. Res. Space Physics*, *120*, 7416–7432, doi:10.1002/2015JA021398.

Yeh, H.-C., J. C. Foster, F. J. Rich, and W. Swider (1991), Storm time electric field penetration observed at mid-latitude, *J. Geophys. Res.*, *96*, 5707–5721, doi:10.1029/90JA02751.

Zhao, H., et al. (2015), The evolution of ring current ion energy density and energy content during geomagnetic storms based on Van Allen Probes measurements, *J. Geophys. Res. Space Physics*, *120*, 7493–7511, doi:10.1002/2015JA021533.